Chapter 19
Estimation of the Lift-to-Drag Ratio Using the Lifting Line Method: Application to a Leading Edge Inflatable Kite

Richard Leloup, Kostia Roncin, Guilhem Bles, Jean-Baptiste Leroux, Christian Jochum, Yves Parlier

Abstract The use of kites for auxiliary propulsion reduces oil consumption for vessels. But the complexity of the kite numerical simulation induces the development of computationally efficient models based on lifting line theory to evaluate the aerodynamic characteristics of the kite. The presented 3D lifting line model takes into account the three-dimensional shape of the kite and the viscosity of the fluid. The proposed model was applied to a *F-one Revolt* Leading Edge Inflatable kite to predict its lift-to-drag ratio. Finally, this method is in very good agreement with CFD simulations in the case of a paragliding wing, but needs a much smaller computational effort.

19.1 Introduction

The need in reducing the CO_2 emissions and the increasing oil prices affect all transportation industries and especially the maritime industry. This induces to redesign propulsion systems of ships to spare energy. In this context, taking advantage of wind energy by using kites as auxiliary propulsion device can be a solution [18]. Projects like those of Skysails or OCEA (project "Beyond the Sea®") can be mentioned. These will lead to develop new concepts with dimensions, loads and stresses in materials never reached before for kites. With increasing size, traditional empirical approaches are becoming too slow and the costs of prototypes too expensive. To help designers to deal with these new challenges, there is a need to develop methods to quickly and efficiently compare several kite solutions in the design loop.

Richard Leloup · Kostia Roncin (✉) · Guilhem Bles · Jean-Baptiste Leroux · Christian Jochum
LBMS (EA 4325), ENSTA-Bretagne, 29806 Brest Cedex 9, France, e-mail: kostia.roncin@ensta-bretagne.fr

Yves Parlier
OCEA, rue des Terres Neuves, BP 21, 33322 Bègles Cedex, France

As a matter of fact, studies on kite have increased significantly during the last decade. The literature provides numerous articles that started to treat flight dynamics [11, 23] flight control [9], structure deformation [4] or aerodynamic forces modeling [16, 17, 24]. One of the first studies on kites and their ability to produce energy was achieved in 1980 [15]. In this study the power delivered by the kite in a stationary flight case is compared to the one obtained in a dynamic flight case. Wellicome and Wilkinson [25] compared also stationary and dynamic flight strategies, but applying them for boat propulsion with the so-called "zero-mass" modeling where the mass of the kite is neglected. Newton's laws were then applied considering only the aerodynamic forces and tethers tensions. For a given true wind speed and position of the kite in the wind window, the equations can be solved to calculate the apparent wind speed and tension in the lines. Using such a modeling, Dadd et al. [6] studied dynamic flight with 8-shaped trajectories, and obtained rather satisfactory comparisons with experimental measurements. Nevertheless, finer approaches have been achieved applying Newton's laws [4, 11, 23]. De Groot [11] applied the Newton's laws to both kites and lines, taking into account the mass distribution.

In the literature, the modeling of aerodynamic forces on a kite was addressed macroscopically by Wellicome and Wilkinson [25] and Dadd [6, 7] where the wing was represented by its general characteristics, like surface, lift coefficient and lift-to-drag ratio. Some authors assumed aerodynamic coefficients [2, 15, 25], or evaluated them by comparison with experimental data [6, 7]. Naaijen [18] valuated the aerodynamic coefficients thanks to calculations on 2D airfoils. Dadd et al. [6] enhanced 2D airfoil predictions by taking into account the three-dimensional effects with the Prandtl formula for an elliptical wing, while Naaijen and Koster [18] enhanced it with the classical lifting line method. Direct calculations on a 3D geometry were also performed either under inviscid flow assumption [3, 5, 10] or through Navier-Stokes simulations as performed by Maneia [16], Maneia et al. [17] or Wachter [24]. For such calculations, the geometry of the kite is typically a defined reference shape [16] or measured by wind tunnel experiments [24].

Taking into account the deformation of the wing, Breukels [4] proposed the most accomplished method today. A fluid structure coupling is done between simulations based on RANS equations for the fluid (Fluent) and a multibody dynamic simulation for the structure (MSC Adams). However heavy resources and computation time associated with this kind of approach, still let room for simpler flight modeling, as those based on the zero-mass assumption adopted even recently [6, 7]. Nonetheless, several key points could be incorporated into the zero mass modeling without compromising excessively its fast implementation. For the simulation of flight dynamics, following physical aspects should be addressed: the three-dimensional geometry of the kite, its deformation, the change in distribution of loads along the kite, the variation of aerodynamic characteristics along a path. The classical lifting line theory of Prandtl [20] can be seen as a good candidate to be used within the zero-mass modeling. This theory was originally dedicated to a straight wing in translation with a planar wake aligned to the relative uniform upstream flow. Following Sivells and Neely [21], the theory can be enhanced to cope with small additional 3D effects regarding the wing geometry (such as little sweep and dihedral angles) and the flight

path (such as little translations perpendicular to the main one or little rotations). One should keep in mind that such enhancements, provided by codes such as XFLR5, are subject to the limitations of lifting line theory and should not be expected to give accurate results for wings of low aspect ratio and large amounts of sweep. In fact, the direct application to 3D kite geometry and flight path requires so crude linearization assumptions that the results are not satisfactory regarding the experiments, in particular in the case of the simulation of a rotating kite which is one of the possible extends of the present work [14].

However, other methods based on the lifting line principle, able to take into account the curvature of a kite, can be developed [12] but still only for high aspect ratio kites. In the present work, a more general method inspired from the works of Phillips and Snyder [19] and Katz and Plotkin [13] has been implemented. The so-called "3D lifting line" applied takes into account the three-dimensional shape, and includes viscosity effects by a boundary layer calculation done with XFOIL.

Consequently, the present paper first described how the 2D kite profile and the 3D shape were measured on a real LEI kite (*F-one Revolt*). The aerodynamic characteristics of the 2D profile were then calculated and integrated in the 3D lifting line model. Validation of the aerodynamic predictions was obtained by comparison with CFD simulations performed by Maneia [16] on a paragliding wing. Finally, the model was applied to the *F-one Revolt* kite to evaluate its lift-to-drag ratio.

19.2 Reference frames and kite apparent wind velocity

The kite apparent wind velocity and direction are given by the "zero mass" model. In this part we define the reference frames which allow to express the apparent wind velocity. This velocity is the input to feed the lifting line model which is presented in Sect. 19.5.

19.2.1 Principle and reference frames

Figure 19.1 shows the kite in the wind window corresponding to a quarter sphere. Point O is the attachment point of the tethers on the ground or on the deck of a ship. The reference frame R_w is attached to this point and oriented so that $\mathbf{x}_w$ remains in the wind direction (or ship apparent wind). $\mathbf{z}_w$ is in the direction of the gravity acceleration. Point K is located at the quarter chord in the symmetry plane of the kite. The reference frame R_{k0}, which is attached to point K, is obtained by rotating about $\mathbf{z}_w$ by the azimuth angle, ϕ , and then by the elevation angle (θ - π / 2) about $\mathbf{y}_{k0}$. Unit vector $\mathbf{x}_{vk}$ corresponds to the direction of the kite velocity and is obtained by rotating vector $\mathbf{x}_{k0}$ about $\mathbf{z}_{k0}$ by angle χ_{vk}. R_b is the body reference frame, attached to the kite. The aerodynamic reference frame R_a is oriented in accordance with the apparent wind velocity in the symmetry plane of the kite as shown in Fig. 19.2.

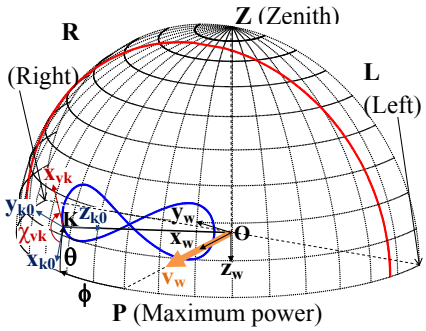

Fig. 19.1 Flying kite within the wind window

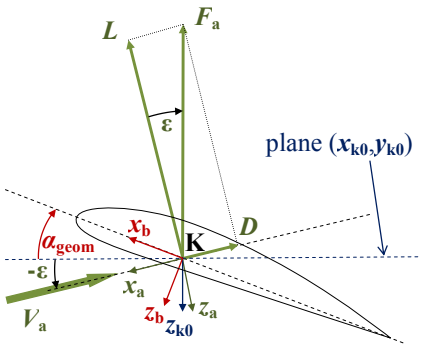

Fig. 19.2 Representations of the glide angle ε and of aerodynamic forces in the symmetry plane of the kite

According to the Newton's laws applied to the kite at point K, assuming that the mass of the kite is zero, we obtain:

$$\mathbf{T} + \mathbf{F}_\mathrm{a} = \mathbf{0} \tag{19.1}$$

The aerodynamic resultant, $\mathbf{F}_\mathrm{a}$, is opposite to the tension in the lines, $\mathbf{T}$, at any time and these two forces are aligned on the same axis that goes from point of attachment O to the kite K. The second equation which governs the kite movement is the apparent wind equation:

$$\mathbf{v}_\mathrm{a} = \mathbf{v}_\mathrm{w} - \mathbf{v}_\mathrm{k} \tag{19.2}$$

19.2.2 Apparent wind velocity expression

By definition of the aerodynamic resultant, we have:

$$\mathbf{F}_\mathrm{a} = \mathbf{L} + \mathbf{D} \tag{19.3}$$

In the plane ($\mathbf{x}_\mathrm{a}$,$\mathbf{z}_\mathrm{a}$), we have the configuration shown in Fig. 19.2. We can also write, by projecting Eq. (19.3) onto the corresponding axes:

$$-F_\mathrm{a}\,\mathbf{z}_{\mathrm{k0}} = -L\,\mathbf{z}_\mathrm{a} - D\,\mathbf{x}_\mathrm{a} \tag{19.4}$$

With

$$L = \frac{1}{2}\rho A v_\mathrm{a}^2 C_\mathrm{L} \tag{19.5}$$

$$D = \frac{1}{2}\rho A v_a^2 C_D = L \tan\varepsilon \tag{19.6}$$

$$F_a = \frac{L}{\cos\varepsilon} \tag{19.7}$$

Where A is the projected kite area and ρ the air density.

Moreover, the equation defining the apparent wind on the kite can also be written by projecting onto the corresponding axes:

$$-v_a\,\mathbf{x}_a = v_w\,\mathbf{x}_w - v_k\,\mathbf{x}_{vk} \tag{19.8}$$

By scalar multiplication of Eq. (19.8) with $\mathbf{z}_{k0}$, we obtained:

$$v_a = -\frac{v_w\,\mathbf{x}_w.\mathbf{z}_{k0}}{\sin\varepsilon} \tag{19.9}$$

The lifting line method was implemented in the case of a kite produced by the *F-one* company (*Revolt* model). Its flat area is equal to 3.76 square meters. The proposed method will be described in this case in the following sections. Particularly, the lifting line method involves a 2D profile of the wing and its aerodynamic characteristics, which both have to be evaluated.

19.3 Aerodynamic characteristics of the LEI kite 2D wing profile

19.3.1 Scan of the wing

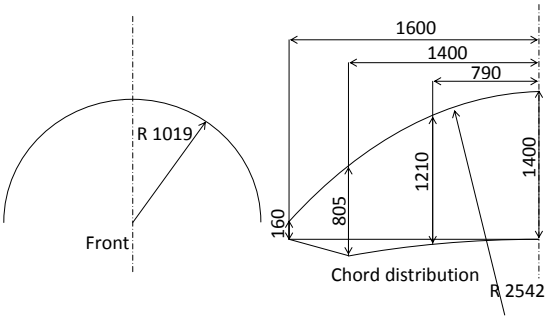

Fig. 19.3 3D geometry of the *F-one Revolt*

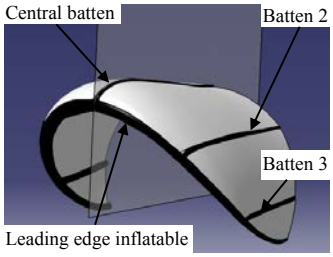

Fig. 19.4 The 3D reconstruction of the LEI kite geometry using a CAD software tool

The LEI kite geometry was measured using a 3D scanner of the GOM company (ATOS model). The kite was put in a position as similar as possible to its flying position. It would have been better if it were in a real flying position, as, for example in [24]. But the flying kite shape can be approximated without wind load assuming that

the shape of a LEI kite is mainly ruled by the geometry of the inflatable battens and leading edge. As a matter of fact, only the inflated battens were used to determine the kite profile. The scattered scanned points were processed using a CAD software tool (CATIA) in order to reconstruct the 3D geometry of the kite (Fig. 19.4). The 2D wing profile was obtained from scanned points along a seam line on the upper side of the middle batten.

19.3.2 Smoothing the scanned profile

The analytical formula of NACA 4 digits is used as a smoothing function for the profile of the LEI kite. The three parameters of the NACA 4 digits foil type [1] were evaluated by the least square method: m = -5.13×10^{-2}, p = 7.35×10^{-1}, t = 33.83×10^{-2}.

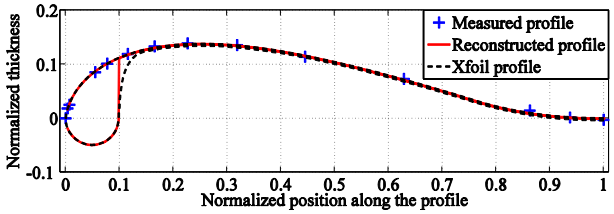

Fig. 19.5 Measured and smoothed profiles

The average difference between the measured and smoothed profiles is 2.2 mm (0.17 % chord) on the central inflatable batten. It is 1.19 % and 2.58 % for the other two battens. To simplify the modeling, the profile is considered to be the same along the whole span. Figure 19.5 shows the superposition of the measured profile and the profile obtained by the least square method.

A semicircle models the lower part of the inflatable leading edge. In order to thicken the rest of the wing, profile is shifted by a distance which represents the thickness of the LEI kite fabric. This modeling induces a tangency discontinuity behind the leading edge (continuous curve in Fig. 19.5). The mesh has been smoothed in order to obtain a good convergence of the calculations of drag and lift coefficients with XFOIL (dashed line).

19.3.3 XFOIL evaluation of lift and drag coefficients

XFOIL models the flow around 2D profiles taking into account the viscosity by coupling potential flow and integral boundary layer [8]. It has been used to determine

the 2D characteristics of the LEI kite sections, as required for the lifting line calculation. The curve of the lift coefficient, as a function of incidence, determines a_0 (lift curve slope) and α_0 (zero lift angle). Furthermore the evolution of the 2D drag coefficient is obtained as a function of incidence and Reynolds number for each section.

For a low aspect ratio wing like a kite, these 2D data can not be directly used to calculate the lift-to-drag ratio because of the importance of the 3D effects. Therefore the lifting line theory was chosen to model the kite.

19.4 3D Lifting line method

19.4.1 Principle

Because the wingspan is finite, the flow generated is three-dimensional. As a matter of fact, near the extremity of a wing, the difference between the pressure at the intrados (high pressure) and at the extrados (low pressure) induces a flow movement from the intrados to the extrados. Qualitatively a secondary flow along the span is superimposed to the principal flow along the chord. This secondary flow is more and more intense close to the wing extremity. In fact the wing extremity creates a deviation of the flow lines towards the tip at the intrados and towards the root at the extrados. Then it creates a vorticity phenomenon which is convected and diffused in the wing wake.

In the lifting line theory of Prandtl [20] the wing is modeled by two vortex systems: the bound vortex along the span, which models the lift of the section, and a sheet of free trailing vortices aligned with the flow, which models the wake, and whose intensities are directly related to the bound vortex through the general circulation conservation theorems (Lagrange, and Kelvin-Helmholtz).

In the present study, a more general method was used inspired by the works of Phillips and Snyder [19] and Katz and Plotkin [13]. According to Phillips, it predicts accurately the effects of both sweep and dihedral as well as the effects of aspect ratio, camber, and planform shape.

19.4.2 Wing modeling

The lifting line method consists in modeling a wing using horseshoe vortices which are composed of two kinds of vortex segments. The first part (bound vortex) models the lifting properties of the wing and is located at quarter of the chord. The second part consisting of two semi-infinite elements (free vortex) models the wake. Each horseshoe vortex is composed of five vortex segments as presented in Fig. 19.6. The wing is then modelled by several horseshoe vortices arranged side by side as shown

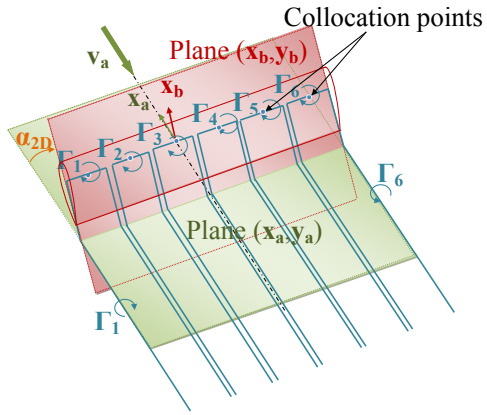

Fig. 19.6 Wing modeling using several horseshoe vortices arranged side by side

in Fig. 19.6. The collocation points are located at half of the bound vortex. Each vortex has a constant circulation equal to Γ_j.

19.5 Apparent wind on each section of the wing

19.5.1 On the middle section

In order to enter the results of the 3D lifting line into the "zero mass" model [6, 7, 14, 25], the kite orientation is defined according to this model. The apparent wind direction is considered to belong to the symmetrical plane of the kite. The apparent wind norm is obtained from the "zero mass" model formula. Then it depends on the kite position within the wind window, on the true wind velocity and on the lift-to-drag ratio. Its expression is given in Eq. (19.9). The central section configuration is shown in Fig. 19.7. The incidence α_{2D} is given by the formula

$$\alpha_{2D} = \alpha_{geom} + \varepsilon \tag{19.10}$$

Thus, the apparent wind velocity and the incidence at kite center depend on the glide angle which is given by the lifting line. An iterative loop is then necessary to ensure that the input glide angle is the same as the output glide angle as presented in the algorithm in Fig. 19.9. The geometric incidence angle is controlled by the kite tethers.

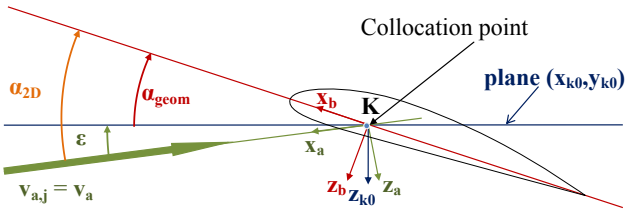

Fig. 19.7 Description of the incidence angle α_{2D} in the kite middle section

19.5.2 Apparent wind on each kite section

A local kite bound reference system $R_{b,j}$ is defined for each section of the kite. $R_{b,j}$ corresponds to a rotation of R_b around $\mathbf{x}_b$ by the angle ζ_j. A local aerodynamic reference system $R_{a,j}$ is also defined. $\mathbf{x}_{a,j}$ is in the direction of the projection of the apparent wind velocity onto the plane $(\mathbf{x}_{b,j},\mathbf{z}_{b,j})$ and $\mathbf{z}_{a,j}$ is perpendicular to $\mathbf{x}_{a,j}$ in the plane $(\mathbf{x}_{b,j},\mathbf{z}_{b,j})$. The incidence angle $\alpha_{2D,j}$ of the section is obtained by projecting the apparent wind velocity $\mathbf{v}_{a,j}$ on each collocation point, in each section plane $(\mathbf{x}_{b,j},\mathbf{z}_{b,j})$.

$$\alpha_{2D,j} = \arctan\left(\frac{\mathbf{v}_{a,j}.\mathbf{z}_{b,j}}{\mathbf{v}_{a,j}.\mathbf{x}_{b,j}}\right) \tag{19.11}$$

19.6 Induced velocity on each collocation point

19.6.1 Definition

On each collocation point j, the free and the bound vortices induce an additional velocity called induced velocity $\mathbf{v}_{ind,j}$. The vector sum of apparent wind velocity and induced velocity at each kite section produces a local relative velocity called effective velocity. The incidence angle is also modified. As presented in Fig. 19.8 this angle called effective angle $\alpha_{eff,j}$ is obtained by subtracting the induced angle $\alpha_{ind,j}$ from the section incidence angle $\alpha_{2D,j}$ [13]:

$$\alpha_{eff,j} = \alpha_{2D,j} - \alpha_{ind,j} \tag{19.12}$$

Where

$$\alpha_{ind,j} = \arctan\left(\frac{\mathbf{v}_{eff,j}.\mathbf{z}_{a,j}}{\mathbf{v}_{eff,j}.\mathbf{x}_{a,j}}\right) \approx -\arctan\left(\frac{\mathbf{v}_{ind,j}.\mathbf{z}_{a,j}}{\mathbf{v}_{a,j}.\mathbf{x}_{a,j}}\right) \approx -\frac{\mathbf{v}_{ind,j}.\mathbf{z}_{a,j}}{\mathbf{v}_{a,j}.\mathbf{x}_{a,j}} \tag{19.13}$$

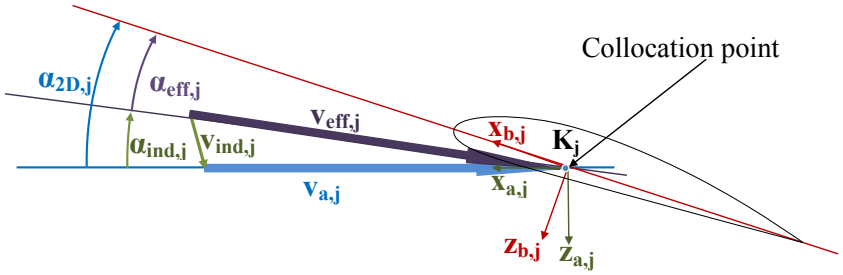

Fig. 19.8 Projection of velocity vectors in a kite section plane

19.6.2 Induced velocity on any point

Each horseshoe vortex is modeled by an addition of vortex segments. The velocity induced by a horseshoe vortex is obtained by summing the velocities induced by each vortex segment [13]. Then, the velocity induced on any point P by a vortex segment situated between points 1 and 2 according to Katz and Plotkin [13] can be written as

$$\mathbf{v}_{\text{ind}} = \frac{\Gamma}{4\pi}\left[(\mathbf{r}_1 - \mathbf{r}_2).\left(\frac{\mathbf{r}_1}{|\mathbf{r}_1|} - \frac{\mathbf{r}_2}{|\mathbf{r}_2|}\right)\right]\frac{\mathbf{r}_1 \wedge \mathbf{r}_2}{|\mathbf{r}_1 \wedge \mathbf{r}_2|^2} \tag{19.14}$$

According to Eq. (19.14), the scalar product of the velocity normal $\mathbf{z}_{a,j}$ by the induced velocity on point j by the horseshoe vortex i, $(\mathbf{v}_{\text{ind,ji}}.\mathbf{z}_{a,j})$ can be written as

$$\mathbf{v}_{\text{ind,ji}}.\mathbf{z}_{a,j} = b_{ji} \times \Gamma_i \tag{19.15}$$

$\mathbf{v}_{\text{ind,j}}.\mathbf{z}_{a,j}$ can be expressed by :

$$\mathbf{v}_{\text{ind,j}}.\mathbf{z}_{a,j} = b_{j1}\Gamma_1 + b_{j2}\Gamma_2 + b_{j3}\Gamma_3 + \ldots + b_{jn}\Gamma_n = \sum_i b_{ji} \times \Gamma_i \tag{19.16}$$

19.7 3D Lifting line solving

19.7.1 Lifting line equation

The lift coefficient as a function of effective incidence is considered to be linear (slope equals to $a_0 = dC_L/d\alpha_{\text{eff}}$). The lifting line can be applied to cambered profiles considering that the zero lift angle is equal to α_0. For each section j, we obtain

$$C_{L,j} = a_0(\alpha_{\text{eff,j}} - \alpha_0) = a_0(\alpha_{2D,j} - \alpha_0 - \alpha_{\text{ind,j}}) \tag{19.17}$$

According to the Kutta-Joukowski theorem, the section lift, $L_{2D,j}$, is

$$L_{2D,j} = \rho v_{eff,j} \Gamma_j \approx \rho v_{a,j} \Gamma_j \tag{19.18}$$

Then, the lift coefficient can be expressed as, c_j being the chord on collocation point j

$$C_{L,j} = \frac{\rho v_{a,j} \Gamma_j}{\frac{1}{2}\rho c_j v_{a,j}^2} = \frac{2\Gamma_j}{c_j v_{a,j}} \tag{19.19}$$

The effective incidence becomes

$$\alpha_{eff,j} = \frac{2\Gamma_j}{c_j v_{a,j} a_0} + \alpha_0 \tag{19.20}$$

Replacing the effective incidence $\alpha_{eff,j}$ and the induced incidence $\alpha_{ind,j}$ by their expressions in equations 19.12 and 19.13 and rearranging the terms, we obtain

$$\Gamma_j - \frac{c_j a_0 v_{a,j}}{2} \times \frac{\mathbf{v}_{ind,j}.\mathbf{z}_{a,j}}{\mathbf{v}_{a,j}.\mathbf{x}_{a,j}} = \frac{c_j a_0 v_{a,j}}{2} (\alpha_{2D,j} - \alpha_0) \tag{19.21}$$

Then, equation 19.21 becomes, in matrix form,

$$\sum_i \left[\delta_{ji} - \frac{a_0}{2} \left(\sum_k D_{jk} \times b_{ki} \right) \right] \times \Gamma_i = \frac{a_0}{2} c_j v_{a,j} (\alpha_{2D,j} - \alpha_0) \tag{19.22}$$

Where

$$j \neq k \Longrightarrow D_{jk} = 0 \tag{19.23}$$

$$j = k \Longrightarrow D_{jj} = \frac{c_j v_{a,j}}{\mathbf{v}_{a,j}.\mathbf{x}_{a,j}} \tag{19.24}$$

By solving this equation, it is possible to obtain the circulation at each collocation point j along the span. The algorithm used to solve the 3D lifting line is presented in Fig. 19.9.

A non linear algorithm was proposed by Phillips and Snyder [19] to solve this equation without our linear approximations in equations 19.13 and 19.18. In the present study, the difference between the linear and the nonlinear solution has been found to be less than 0.1%. Consequently, the linear formulation has been employed because it is simpler and faster.

19.7.2 Calculation of the kite aerodynamic characteristics

By solving Eq. (19.22) the circulation along the span is obtained. It is then possible to calculate the lift at each collocation point following Eq. (19.18), and the total lift $\mathbf{L}$ is obtained by integrating the 2D lift, $\mathbf{L}_{2D}$, along the span b.

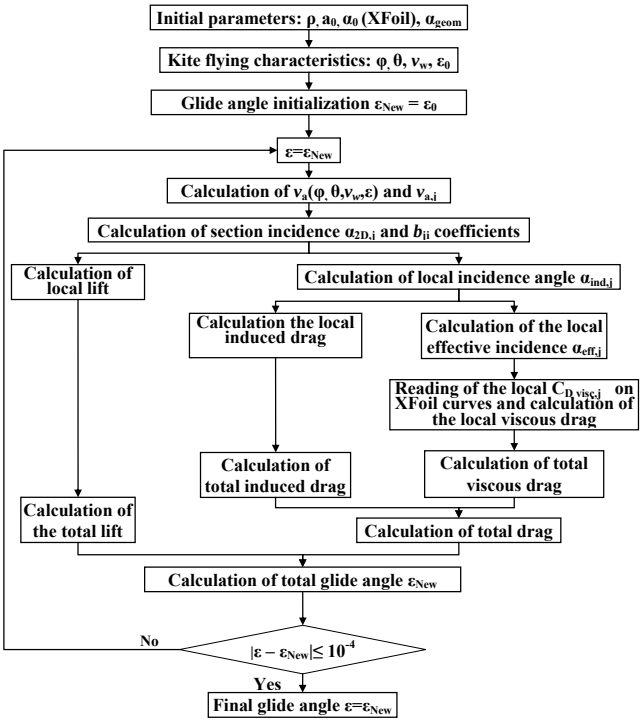

Fig. 19.9 3D Lifting line algorithm

$$\mathbf{L} = \int_{-\frac{b}{2}}^{+\frac{b}{2}} \mathbf{L}_{2\mathrm{D}}(s)ds \tag{19.25}$$

The induced drag is obtained in the same manner. Knowing the effective incidence, the viscous drag is then calculated using the XFOIL curves. The glide angle, ε, is thus simply calculated:

$$\varepsilon = \arctan\left(\frac{|\mathbf{D}|}{|\mathbf{L}|}\right) \tag{19.26}$$

19.8 Comparison of the lifting line and Navier-Stokes methods in the case of a paragliding wing

In order to verify the lifting line method on a curved wing like a kite, the results are compared to those obtained by Maneia [16] using the Navier-Stokes software tool STAR-CCM+ for a paragliding wing. The wing was modeled by extruding a Clark

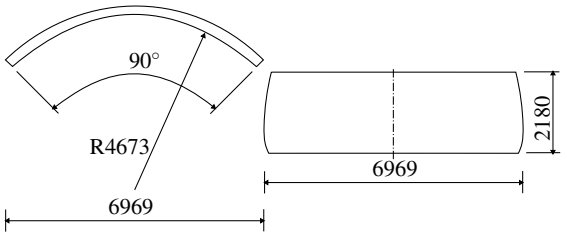

Fig. 19.10 3D geometry of the paragliding wing studied in [16]

Y profile along the curved span. The 3D geometry studied is presented in Fig. 19.10 and reproduced in the lifting line model.

To compare the results, the aerodynamic characteristics of the profile were not taken from the experimental profile curves but from the 2D CFD curves of the wing by Maneia [16]. The lift and drag coefficients were obtained by Maneia using the Spalart-Allmaras turbulence model [22]. Knowing the evolution of the lift coefficient as a function of incidence, it is possible to calculate the values of the lift coefficient slope a_0 (5.99 rad^{-1}) and the zero lift angle α_0 (-5.48 °) of the profile. The lifting line model was applied to the paragliding wing geometry in order to compare the results. Finally, the evolution of the whole wing lift and drag coefficients are obtained as functions of incidence.

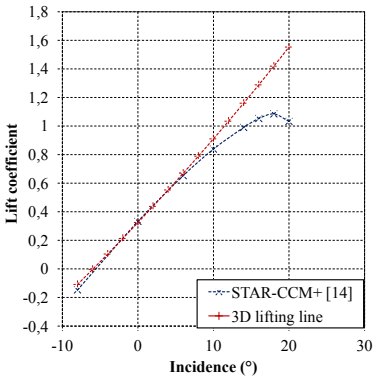

Fig. 19.11 Comparison between the lift coefficients obtained by the 3D lifting line and CFD [16] methods

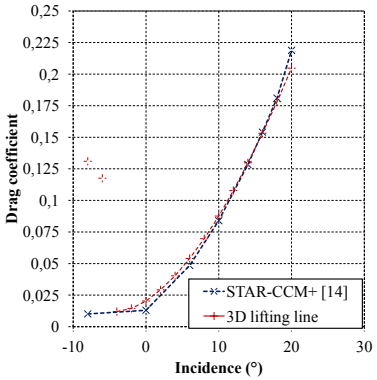

Fig. 19.12 Comparison between the drag coefficients obtained by the 3D lifting line and CFD [16] methods

It can be observed in Fig. 19.11 that the lifting line gives good results in comparison with Navier-Stokes calculations regarding lift coefficient in the linear part. Nevertheless we see also the limitations of the linear modeling that does not give good result near the stall point. Instead, Fig. 19.12 shows that the drag coefficient is well predicted until 20 ° of angle of attack, even beyond the stall point. This can be explained in the following manner. The linear modeling overestimates the lift coef-

ficient in the stall region, consequently overestimating the induced drag, the local vortex circulation and the induced angle of attack α_{ind} (Fig. 19.8). Subsequently the resulting effective angle of attack α_{eff} and therefore the viscous drag are underestimated in the stall zone. At last the two errors compensate each other leading to rather unexpected good results. Two outliers, for -6 ° and -8 ° angle of attack, highlight the limitations of using XFOIL. For such values, the separation zone becomes too large and can not be reattached onto the intrados. Fortunately, these angles are not expected to be achieved in a normal operating range of the wing.

19.9 Lifting line method applied to a LEI kite

The lifting line described before has been applied on an *F-one Revolt* LEI kite, whose characteristics are presented on table 19.1. These data were obtained thanks to the measurements performed on the *F-one Revolt* kite and its digital reconstruction presented in Sect. 19.3. The chord distribution was measured on the real kite unfolded on the ground. Furthermore, the kite is considered to have a semi-circular shape, as shown in Fig. 19.3, whose radius was obtained thanks to laser measurements.

Characteristic	Value
Total span	3.6 m
Projected surface	2.77 m^2
Lift coefficient slope a_0	6.73 rad^{-1}
Zero lift angle α_0	-5.65 °

Table 19.1 *F-one Revolt* LEI kite characteristics

It is then possible to get the lift and drag distribution along the span and the total lift and drag by integration along the span. The geometric incidence angle α_{geom} (Fig. 19.2) is adjusted in order to equal the lift coefficient experimental value of 0.776 by Dadd et al. [6]. At last, we obtain the values presented on table 19.2 and compared to those measured experimentally on a similar kite [6, 7].

	Classical lifting line (Projected)	XFLR5 lifting line (Unfolded)	Present 3D lifting line	Experimental (Dadd [6, 7])
Glide angle ε	15.32 °	7.0 °	7.62 °	9.55 ± 0.63 °
Drag coefficient	0.212	0.095	0.104	0.128 ± 0.012

Table 19.2 Comparison between 3D lifting line and experimental measurements for a lift coefficient of 0.776

Table 19.2 presents the results for three variations of the lifting line method. The classical lifting line method developed by Prandtl which does not take into account the sweep neither the dihedral of the wing, is firstly applied on the projected surface. The open source code XFLR5 uses the same method with, in addition, a non linear treatment of the lift coefficient [21]. But it uses the unfolded surface instead of the projected one. At last, the present "3D lifting line" method allows to take into account both sweep and dihedral. It can be seen that she gives the best results regarding the experiments of Dadd. On one side, considering the projected area, the classical method is too pessimistic. On another side, considering the unfolded area, it is too optimistic.

Although the *Flexifoil Blade III* whose aerodynamic characteristics were measured by Dadd et al. [6] has approximately the same dimensions as the *F-one Revolt* kite, some differences can explain that we do not obtain exactly the same aerodynamic characteristics. On one hand, the leading edge of a ram-air kite like the *Flexifoil blade III* is composed of several inlets. These inlets generate an additional drag. Moreover, the flying shape of a ram-air kite is ensured by a set of numerous lines. These lines also generate an additional drag which is not further taken into account in our calculation. On the other hand, the influence of the inflatable leading edge of a LEI kite like the *F-one Revolt* is taken into account by the XFOIL calculations. In addition, the flying shape of a LEI kite is maintained by the inflatable structure, thereby needing fewer lines and less associated drag than a ram-air kite. Thus, these differences may partly explain the fact that the drag calculated by the 3D lifting line on the *F-one Revolt* kite is lower than the one measured by Dadd on the *Flexifoil blade III*.

19.10 Discussion

With similar results to simulations based on RANS equations at limited angles of attack (Fig. 19.11, Fig. 19.12), lifting line method takes its advantage from demanding less computer resources and calculation time. Thus a lifting line calculation could be done at each point of the trajectory of the "zero-mass" model which is practically too long with a CFD software tool like STARCCM+.

The 3D lifting line model presented could further be improved by considering the non-linearity of the lift coefficient as a function of the incidence angle. An unsteady lifting line model with Lagrangian wake modeling could also be integrated into the proposed model in order to capture more precisely the geometry of the wake and its influence on aerodynamic loading.

Furthermore, it would be better to compute the flying shape of the *F-one Revolt* kite in order to have a better definition of the kite geometry and its evolution with the aerodynamic loading during the flight. This could be done using a fluid-structure interaction analysis in a further work. In fact, the 3D lifting line model gives the effective incident velocity field of each section. So the effective pressure distribution can be calculated, and these loads could be applied to a 3D finite-element structural

model of the kite; such FEM model would allow to predict the deformation of the kite geometry and stresses into the fabrics and seams. Then, a fluid-structure interaction analysis of a flying kite would be possible to determine the aerodynamic characteristics of the flying shape of the *F-one Revolt* kite.

19.11 Conclusion

A 3D lifting line model was applied in the present study with the aim to predict the aerodynamic characteristics during a kite flight with a fast relevant numerical calculation. The presented model takes into account the real 3D geometry of the kite, i.e. kite sweep, dihedral and camber. The 3D geometry of an *F-one Revolt* LEI kite was measured by means of an optical 3D laser scanner (GOM). The lift and drag coefficients of this 3D geometry were obtained by the proposed 3D lifting line model.

The aerodynamic characteristics of the 2D profile are evaluated using XFOIL that couples potential flow and integral boundary layer [8], thus taking into account the viscosity of the fluid. The proposed model was compared with simulations based on RANS equations in the case of a paragliding wing [16]. The two methods are in good agreement in the linear part for limited angles of attack.

Acknowledgements The authors thank Frédéric Montel for his help during the kite 3D scanning and Michel Jaffrès for the CAD reconstruction.

References

1. Abbott, I. H., Doenhoff, A. E.: Theory of wing sections. Dover Publications (1959)
2. Argatov, I., Rautakorpi, P., Silvennoinen, R.: Estimation of the mechanical energy output of the kite wind generator. Renewable Energy **34**(6), 1525–1532 (2009). doi: 10.1016/j.renene.2008.11.001
3. Baayen, J. H.: Vortexje - An Open-Source Panel Method for Co-Simulation. Submitted (2012). arXiv:1210.6956 [cs.DS]
4. Breukels, J.: An Engineering Methodology for Kite Design. Ph.D. Thesis, Delft University of Technology, 2011. http://resolver.tudelft.nl/uuid:cdece38a-1f13-47cc-b277-ed64fdda7cdf
5. Chatzikonstantinou, T.: Numerical analysis of three-dimensional non rigid wings. AIAA Paper 89-0907. In: Proceedings of the 10th Aerodynamic Decelerator Conference, Cocoa Beach, FL, USA, 18–20 Mar 1989. doi: 10.2514/6.1989-907
6. Dadd, G. M., Hudson, D. A., Shenoi, R. A.: Comparison of two kite force models with experiment. Journal of Aircraft **47**(1), 212–224 (2010). doi: 10.2514/1.44738
7. Dadd, G. M., Hudson, D. A., Shenoi, R. A.: Determination of kite forces using three-dimensional flight trajectories for ship propulsion. Renewable Energy **36**(10), 2667–2678 (2011). doi: 10.1016/j.renene.2011.01.027
8. Drela, M.: Two-dimensional transonic aerodynamic design and analysis using the Euler equations. Ph.D. Thesis, Massachusetts Institute of Technology, 1985

9. Fagiano, L.: Control of tethered airfoils for high-altitude wind energy generation. Ph.D. Thesis, Politecnico di Torino, 2009. http://lorenzofagiano.altervista.org/docs/PhD_thesis_Fagiano_Final.pdf
10. Gaunaa, M., Paralta Carqueija, P. F., Réthoré, P.-E. M., Sørensen, N. N.: A Computationally Efficient Method for Determining the Aerodynamic Performance of Kites for Wind Energy Applications. In: Proceedings of the European Wind Energy Association Conference, Brussels, Belgium, 14–17 Mar 2011. http://windenergyresearch.org/?p=1557
11. Groot, S. G. C. de, Breukels, J., Schmehl, R., Ockels, W. J.: Modeling Kite Flight Dynamics Using a Multibody Reduction Approach. AIAA Journal of Guidance, Control and Dynamics **34**(6), 1671–1682 (2011). doi: 10.2514/1.52686
12. Jackson, P. S.: Optimal Loading of a Tension Kite. AIAA journal **43**(11), 2273–2278 (2005). doi: 10.2514/1.3543
13. Katz, J., Plotkin, A.: Low-speed aerodynamics. 2nd ed. Cambridge University Press (2001)
14. Leloup, R., Roncin, K., Leroux, J.-B., Bles, G., Jochum, C., Parlier, Y. et al.: Estimation par la méthode de ligne portante de l'effet d'un virage sur la finesse: application aux cerfs-volants de traction pour la propulsion auxiliaire des navires. In: Proceedings 13eme Journées de l'Hydrodynamique, Chatou, France, 21–23 Nov 2012. http://website.ec-nantes.fr/actesjh/images/13JH/Articles/Leloup_JH13.pdf
15. Loyd, M. L.: Crosswind kite power. Journal of Energy **4**(3), 106–111 (1980). doi: 10.2514/3.48021
16. Maneia, G. M.: Aerodynamic study of airfoils and wings for power kites applications. M.Sc.Thesis, Politecnico di Torino, 2007. http://maneia.com/doc/MasterThesisManeia.pdf
17. Maneia, G., Tribuzi, C., Tordellac, D., Iovieno, M.: Aerodynamics of a rigid curved kite wing. Submitted to Renewable Energy (2013). arXiv:1306.4148v1 [physics.flu-dyn]
18. Naaijen, P., Koster, V.: Performance of auxiliary wind propulsion for merchant ships using a kite. In: Proceedings of the 2nd International Conference on Marine Research and Transportation, pp. 45–53, Naples, Italy, 28–30 June 2007. http://www.icmrt07.unina.it/Proceedings/Papers/c/26.pdf
19. Phillips, W. F., Snyder, D. O.: Modern adaptation of Prandtl's classic lifting-line theory. Journal of Aircraft **37**(4), 662–670 (2000). doi: 10.2514/2.2649
20. Prandtl, L.: Tragflügeltheorie. I. Mitteilung. Nachrichten von der Gesellschaft der Wissenschaften zu Göttingen, Mathematisch-Physikalische Klasse, 451–477 (1918). http://resolver.sub.uni-goettingen.de/purl?GDZPPN002505223
21. Sivells, J. C., Neely, R. H.: Method for calculating wing characteristics by lifting-line theory using nonlinear section lift data. NACA Technical Note 1269, Langley Memorial Aeronautical Laboratory, Langley, VA, USA, Apr 1947. http://www.dtic.mil/dtic/tr/fulltext/u2/a801339.pdf
22. Spalart, P., Allmaras, S.: A one-equation turbulence model for aerodynamic flow. AIAA Paper 92-0439. In: Proceedings of the 30th Aerospace Sciences Meeting and Exhibit, Reno, NV, USA, 6–9 Jan 1992. doi: 10.2514/6.1992-439
23. Terink, E. J., Breukels, J., Schmehl, R., Ockels, W. J.: Flight Dynamics and Stability of a Tethered Inflatable Kiteplane. AIAA Journal of Aircraft **48**(2), 503–513 (2011). doi: 10.2514/1.C031108
24. Wachter, A. de: Deformation and Aerodynamic Performance of a Ram-Air Wing. M.Sc.Thesis, Delft University of Technology, 2008
25. Wellicome, J. F., Wilkinson, S.: Ship Propulsive Kites - An Initial Study, University of Southampton, Department of Ship Science, 1984. http://hdl.handle.net/10068/658907